Available online at www.sciencedirect.com
SCIENCE DIRECT®
Journal of Nuclear Materials 329–333 (2004) 761–765
journal of nuclear materials
www.elsevier.com/locate/jnucmat

Desorption of helium from austenitic stainless steel heavily bombarded by low energy He ions

M. Tokitani [a,*], M. Miyamoto [a], K. Tokunaga [b], H. Iwakiri [b], T. Fujiwara [b], N. Yoshida [b]

[a] *Interdisciplinary Graduate School of Engineering Science, Kyushu University, Kasuga, Fukuoka 816-8580, Japan*
[b] *Research Institute for Applied Mechanics, Kyushu University, Kasuga, Fukuoka 816-8580, Japan*

Abstract

To discuss helium in the fusion reactor environment, we need more information at much higher doses where the accumulation of helium atoms by implantation in the wall material and the loss by sputtering erosion are at least in balance. In the present work, the behavior of implanted helium in 304SS at high dose was studied by means of in situ microstructure observation and thermal desorption spectroscopy (TDS). TDS experiments showed that helium desorption below about 500 K increased drastically and the total retention saturated at the fluence above 1×10^{21} He/m^2. At this condition a remarkable amount of helium was released even at room temperature with a decay time of 1.7×10^4 s. The microscopic observations lead to the conclusion that helium desorbed in the low-temperature region are detrapped from rather weak trapping sites such as the heavily distorted lattice in the vicinity of highly pressurized bubbles, and other lattice defects, but not from the bubbles themselves.

1. Introduction

The first wall of fusion reactors suffer heavy bombardment of helium particles generated by the D–T fusion reaction. Serious damage by helium has been observed in specimens placed on the first wall position of high temperature plasma confinement devices. In TRIAM-1M for example, very dense dislocation loops and helium bubbles were formed in tungsten and molybdenum exposed to helium plasma discharges for only 125 s [1].

Undesired helium desorption often occurred in the large helical device (LHD) after helium glow discharge cleaning (He-GDC), in which the first wall is made of stainless steel. It was reported that for helium plasma discharge experiments in the LHD, about half of the inlet helium was trapped in the wall, even after a long He-GDC, where the retention of helium is expected to have saturated [2,3]. These results indicate that understanding and control of retention and desorption of helium in first-wall materials is crucial for plasma confinement.

On the other hand, strong irradiation effects of helium have been observed in many kinds of metals such as tungsten and molybdenum including stainless steel [4–6]. It should be noted that bubbles and other type of defects are formed even by irradiation with low energy helium, which is insufficient for displacement of target atoms. We can expect that heavy irradiation damage occurs commonly in many kinds of metals including stainless steels.

In the present work, therefore, the behavior of implanted helium in austenitic stainless steel (304SS) was studied by means of thermal desorption spectroscopy (TDS), scanning electron microscopy (SEM) and transmission electron microscopy (TEM) focusing on the phenomenon at high dose.

* Corresponding author. Tel.: +81-92 583 7719; fax: +81-92 583 7690.
E-mail address: tokitani@riam.kyushu-u.ac.jp (M. Tokitani).

0022-3115/$ - see front matter © 2004 Elsevier B.V. All rights reserved.
doi:10.1016/j.jnucmat.2004.04.177

2. Experimental procedures

Mechanically and electrochemically polished samples of 304SS with the dimensions of $10\times10\times0.1$ mm^3 were prepared for the TDS experiments. They were irradiated with 2 keV-He^+ at room temperature up to a dose of 1×10^{22} He/m^2, where the saturation of helium retention is expected. The ion beam flux was about 1×10^{18} He/m^2 s. After transfer of the sample to the TDS apparatus, thermal desorption of helium was measured with a quadrupole mass spectrometer (QMS) by heating up to 1473 K with a ramping rate of 1 K/s. Long-term desorption by keeping at room temperature was also measured.

The effects of annealing on surface morphology were also examined by means of SEM. Samples irradiated to 1×10^{22} He/m^2 were annealed up to 1473 K in a stepwise fashion (100 or 200 K steps for 10 min). After annealing at each step, the sample was rapidly cooled to room temperature and observed by SEM.

Furthermore, in situ observation under helium ion irradiation was carried out using a TEM equipped with a low energy ion gun to systematically investigate the relationship between helium desorption and the damage structure [7]. Pre-thinned vacuum-annealed 304SS specimens of 3 mm diameter were irradiated with 2 keV-He^+ up to 1×10^{22} He/m^2. The stepwise annealing procedure was also carried out in the TEM to follow damage structure evolution.

3. Results and discussion

3.1. Formation of defects and thermal desorption of helium

The microstructural evolution of 304SS at room temperature under irradiation with 2 keV-He^+ ions is shown in Fig. 1. The upper series of micrographs are bright field images with small deviation parameter s, which fits for observation of defects with strong lattice distortion such dislocation loops and helium platelets. Defects with a strong black image, mainly dislocation loops, appear at first in the early stage of irradiation (1×10^{20} He/m^2). Dislocation loops grow and finally form tangled dislocation networks with increasing dose. On the other hand, very dense helium bubbles of about 1–2 nm in diameter became visible above 1×10^{21} He/m^2 and gradually grow with increasing dose.

Thermal desorption spectra of helium obtained from 304SS specimens irradiated at room temperature with 2 keV-He^+ to doses ranging from 1×10^{19} to 1×10^{22} He/m^2 are plotted in Fig. 2. It is remarkable that the desorption rate in a low-temperature region ($\sim$400 K) increases rapidly above 1×10^{21} He/m^2. In Fig. 3, the total amount of retained helium is plotted against helium dose. It is clear that almost 100% of implanted helium is retained at lower doses but retention saturates above about 1×10^{21} He/m^2. One should note that the detailed desorption spectrum, namely nature of trapped states, changes with increasing the dose from 1×10^{21} to 1×10^{22} He/m^2 (see Fig. 2). The following mechanisms were proposed about irradiation process.

At the beginning of the irradiation, most of the helium is trapped in the radiation induced vacancies and form vacancy–helium complexes. Because of the very strong binding energy of the complex, thermal detrapping of helium occurs at very high temperature, around 1000 K (see 1×10^{19} He/m^2 in Fig. 2). Due to the very high damage rate, about 0.003 dpa/s on average for the dose of 1×10^{18} He/m^2 s, low thermal migration of vacancies and vacancy–helium complexes, and low possibility of recombination of a vacancy–helium complex with an interstitial, the concentration of the vacancy–helium complexes in the damaged area increases

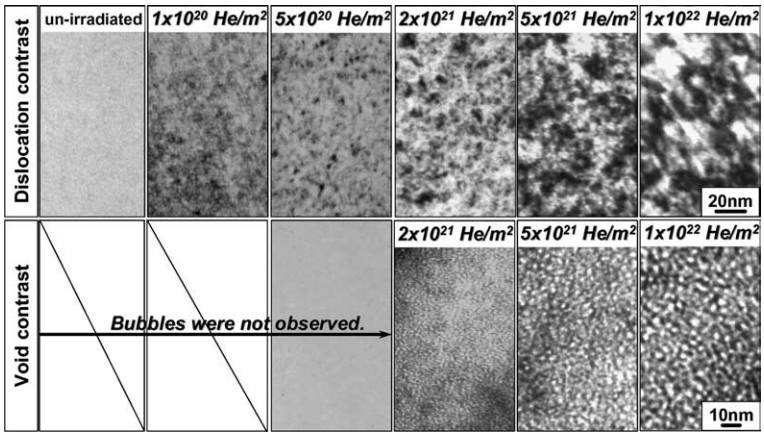

Fig. 1. Microstructural evolution in 304SS during helium ion irradiation ($\sim1\times10^{22}$ He/m^2) at room temperature with energies of 2 keV. Black images show dislocation loops (upper series). White contrasts show helium bubbles (lower series).

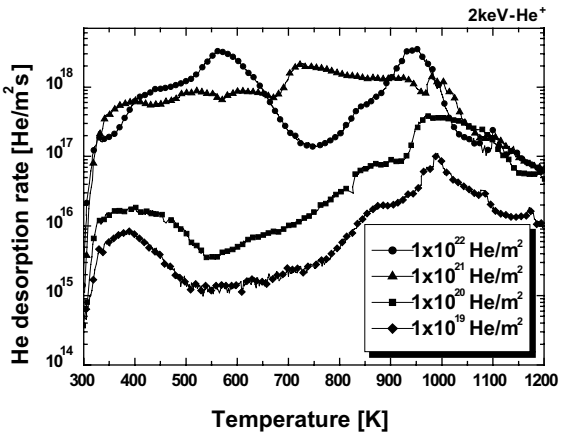

Fig. 2. Thermal desorption spectra of helium obtained from the 304SS specimens irradiated with 2 keV-He^+ for dose ranging from 1×10^{19} to 1×10^{22} He/m^2 at room temperature.

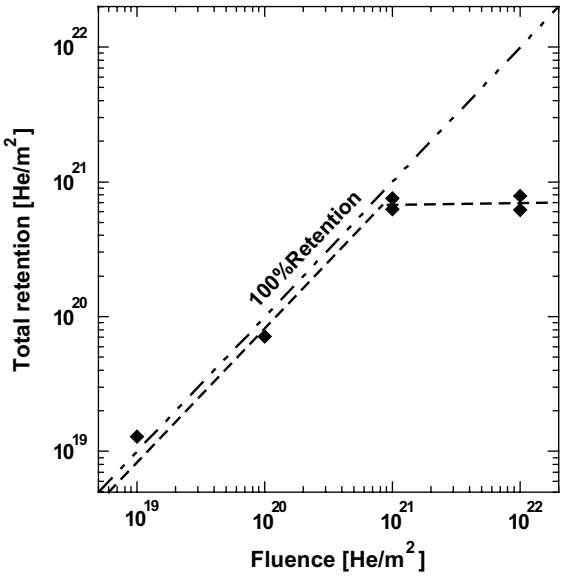

Fig. 3. Total retention of helium in 304SS as a function of helium fluence.

almost linearly and reaches saturation (order of 0.1 at%) at a dose level of about 10^{19} He/m^2. Above this dose level the complexes start to aggregate by an athermal process such as radiation induced diffusion, and form larger vacancy–helium complexes gradually. Injected helium atoms are trapped in these bubbles and finally form bubbles filled with them, which probably occurs around 10^{20} He/m^2. Slow aggregation of the fine bubbles continues and reaches observable size in the TEM at a level of 10^{21} He/m^2 as shown in Fig. 1. Above this dose level, additional trapping of helium atoms by helium bubbles becomes difficult and thus most of the newly injected helium can escape to the surface. Some injected helium is weakly trapped in the distorted lattice around high-pressure bubbles and other types of lattice defects at doses above 1×10^{21} He/m^2. It is likely that these changes in helium trapping result in an increase of de-trapping at low temperatures and saturation of total retention as shown in Figs. 2 and 3.

3.2. Desorption of helium at room temperature

After transporting the sample into the TDS chamber, a quadruple mass spectroscopy measurement was performed keeping the sample at room temperature. The desorption rate of helium is plotted in Fig. 4 against time. The time evolution of the helium desorption rate for 1×10^{21} and 1×10^{22} He/m^2 were fit by the following equation where two desorption processes with different decay constants were assumed.

$$y = A_1 e^{-t/\tau_1} + A_2 e^{-t/\tau_2},$$

where $A_{1,2}$, t, $\tau_{1,2}$ and y are constant, lapsed time, decay constant and desorption late of helium, respectively. The best fitted decay constants are 7.7×10^2 s for the initial rapid desorption and 1.7×10^4 s for the long-term slow desorption. If we adopt these data for the LHD, the desorption rate of helium after 24 h ending of He-GDC is estimated to be about 1.3×10^{-5} Pa m^3/s assuming uniform desorption from the whole vacuum vessel wall (700 m^2). These results indicate that the retention and desorption of helium is a very important issue for plasma confinement devices with a stainless steel wall,

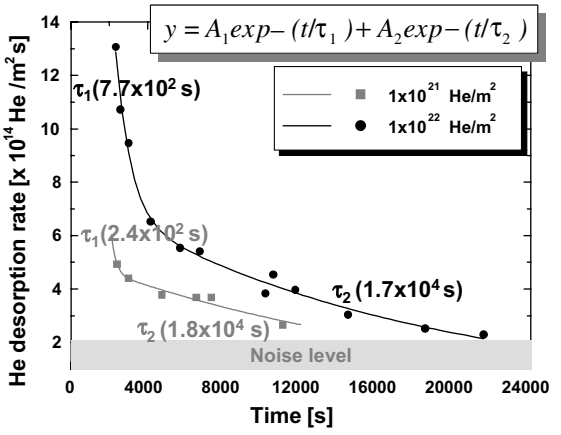

Fig. 4. Desorption rate of the irradiated helium into 304SS at room temperature measured by quadruple mass spectroscopy (symbols). Solid lines are fitting of the experimental data. It was found that remarkable desorption of helium with short decay constant and long decay constant occurred even at room temperature.

and probably even for those with other type of metals such as tungsten due to the similar behavior of helium as mentioned in Section 1.

3.3. Annealing effect

Fig. 5 shows the change of microstructure and surface morphology of the samples irradiated at room temperature with 2 keV-He^+ ions to a dose of 1×10^{22} He/m^2 and stepwise annealed up to 1073 K. The TDS spectrum of helium is also shown for comparison. The spectrum has roughly four desorption peaks as denoted in the figure, #1 (300–450 K), #2 (500–700 K), #3 (850–1050 K) and #4 (1100 K$\sim$). Taking into account the TDS data, coupled with the SEM and TEM observations, we can propose the following mechanisms for the annealing processes.

(1) No remarkable change of bubbles at desorption peak #1 indicates the helium atoms which are rather weakly trapped in the distorted lattice, probably around bubbles, small vacancy–helium complex and other types of defects such as dislocation loops, are released at this stage [4,5]. It seems that helium desorbed by these mechanisms cause the fast and slow desorption at room temperature shown in Fig. 4. To confirm the idea that the weakly trapped helium exists outside of the bubbles, the amount of helium trapped in the high-pressure bubbles was estimated. It is known that the size of gas bubbles increase by emitting interstitial type dislocation loops or by inter-bubble fracture. In the case of the inter-bubble fracture, which is actually observed at 473 K as described later, the critical inner gas pressure P_F for crack formation is given as following [8].

$$P_F \geqslant \frac{2\gamma}{r} + \sigma_f\{(\pi r^2 c^{\frac{2}{3}})^{-1} - 1\},$$

where σ_f, r, c and γ are the theoretical fracture strength of the material, bubble radius, volume density and surface energy of the bubble, respectively. By putting the experimental data at 1×10^{22} He/m^2, $2r_{av} = 1.5$ nm, into the equation, 5.5 GPa is obtained for P_F. This means that the number of helium atoms in a bubble is 1700 and therefore the total of helium retained in the bubbles is 7.9×10^{19} He/m^2. On the other hand, the total amount of retained helium estimated from TDS data experiment was 7.1×10^{20} He/m^2. It means that about 80–90% of the retained helium was trapped outside the bubbles. Although the estimation is rough, the result is nevertheless helpful for understanding the mechanism of the weak trapping. (2) At #2 (500–700 K) stage, helium bubbles start to coalescence and increase their size with increasing temperature. Taking into account the vacancies are already sufficiently mobile at this temperature range, a possible mechanism of this stage is the following. By absorbing thermally mobile small vacancy–helium complexes the small bubbles start to grow and once the neighboring bubbles touch each other their size increases quickly. Due to the increase of inner pressure with increasing temperature, growth by loop punching and by inter-bubble fracture [8,9] can be expected. In reality, the sudden growth of nano-size bubbles was often observed during annealing at 473 K. With increasing temperature, even larger bubbles become mobile and their size increases by aggregating with each other. These phenomena were directly observed during in situ observation at 673 K. It is likely that helium is

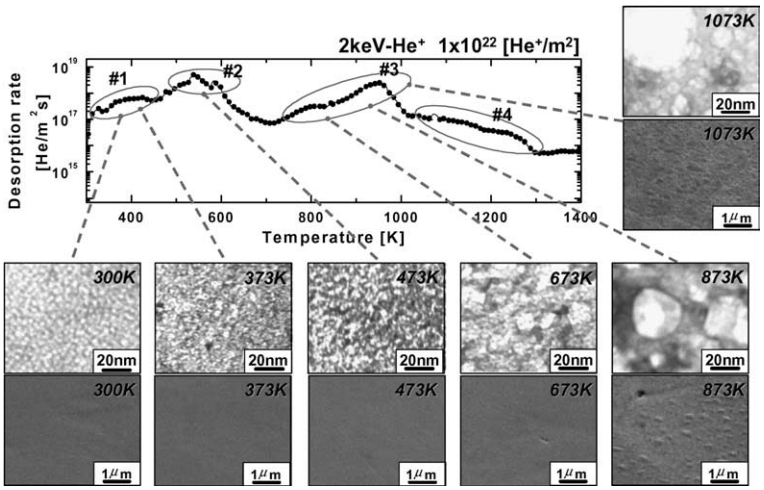

Fig. 5. Change of damage structure and surface morphology in 304SS during isochronal annealing after irradiation ($\sim1\times10^{22}$ He/m^2) at room temperature with 2 keV-He^+. The specimens were annealed for 10 min at each temperature. Upper series: TEM images showing damage structure. Lower series: SEM image showing surface morphology. Corresponding TDS spectrum is also shown for comparison.

released from the bubbles reaching the surface. (3) Bubbles grow larger and form blisters as shown in SEM micrographs at 873 K. These blisters rupture at 1073 K as shown in the SEM micrographs. It seems that formation and breaking of the blisters resulted in the #3 desorption stage. (4) One should note that large helium bubbles remain even after the annealing at 1073 K. It appears that the migration of bubbles to the surface and/or direct detrapping from them one responsible for the helium desorption above 1100 K (#4 stage).

4. Summary

The behavior of implanted helium at high doses in 304SS was studied and the following conclusions were obtained. Very dense helium bubbles of about 1–2 nm in diameter become visible by TEM above 1×10^{21} He/m^2 and gradually grow with increasing dose. When the helium dose exceeds 1×10^{21} He/m^2, the desorption rate in a low-temperature region (#1 stage) increases rapidly. It is likely that this desorption occurs by the detrapping of helium trapped in the distorted lattice around defects such as high-pressure helium bubbles. In the case of heavy irradiation, a remarkable rapid and slow desorption of helium was observed even at room temperature. The decay constants were estimated to be 7.7×10^2 and 1.7×10^4 s. These results indicate that low-temperature desorption of helium will have serious consequences for the operation of plasma confinement devices. It is thought that growth and thermal migration of bubbles play an important role for desorption of helium from 304SS.

References

[1] N. Yoshida, M. Miyamoto, K. Tokunaga, H. Iwakiri, H. Wakimoto, T. Fujiwara, The TRIAM Group, Nucl. Fusion 43 (2003) 655.
[2] H. Suzuki, N. Ohyabu, A. Komori, T. Morisaki, S. Masuzaki, J. Miyazawa, R. Sakamoto, M. Shoji, M. Goto, S. Morita, Y. Kubota, O. Motojima, The LHD Experimental Group, J. Nucl. Mater. 313–316 (2003) 297.
[3] M. Miyamoto, M. Tokitani, K. Tokunaga, T. Fujiwara, N. Yoshida, S. Masuzaki, A. Komori, J. Nucl. Mater., these proceedings.
[4] H. Iwakiri, K. Yasunaga, K. Morishita, N. Yoshida, J. Nucl. Mater. 283–287 (2000) 1134.
[5] N. Yoshida, Y. Hirooka, J. Nucl. Mater. 258–263 (1998) 173.
[6] K. Ono, K. Arakawa, M. Oohashi, H. Kurata, K. Hojou, N. Yoshida, J. Nucl. Mater. 283–287 (2000) 210.
[7] T. Muroga, R. Sakamoto, M. Fukui, N. Yoshida, T. Tsukamoto, J. Nucl. Mater. 196–198 (1992) 1013.
[8] J.H. Evans, J. Nucl. Mater. 76&77 (1978) 228.
[9] G.W. Greenwood, A.J.E. Foreman, D.E. Rimmer, J. Nucl. Mater. 4 (1959) 305.